Negative-muon capture in ionic compounds and some related elements*

L. F. Mausner† and R. A. Naumann
Princeton University, Princeton, New Jersey 08540

J. A. Monard‡ and S. N. Kaplan
University of California, Lawrence Berkeley Laboratory, Berkeley, California 94720

(Received 12 July 1976)

Relative muon capture probabilities for the individual elements of compounds and relative muonic x-ray intensities have been measured for a series of ionic solids and some related elements. Marked similarities are observed in relative K- and L-series intensities of a single ionic species, independent of bond partner (e.g., Cl^- in NaCl and $CaCl_2$). However, significant K-series differences are observed for an element in an ionic vs a covalent situation (e.g., Cl in NaCl and in $NaClO_4$), with the higher K x rays from the covalently bound element showing relative enhancements of as much as a factor of 2 over the ion. The measured intensities have been compared to the predictions of a meson cascade code, which allows variation in the muon initial principal quantum number (N_μ) and the parameter α in the commonly used modified statistical angular momentum distribution, $P(l) = (2l+1)e^{\alpha l}$. The fit was quite insensitive to the choice of N_μ (in the neighborhood $N_\mu = 17$), but the results could not be well fitted with a single value of α. The atomic capture probabilities predicted by recent calculations do not fit the data noticeably better than the Fermi-Teller "Z law."

I. INTRODUCTION

The results of many diverse experiments[1-6] now indicate that the molecular or atomic structure of matter significantly influences the capture of negative mesons. Generally these studies have been nonsystematic and the measurements of x-ray intensities contained large experimental uncertainties. Theoretical work on the deceleration and atomic capture of mesons[7-10] with subsequent radiative and Auger deexcitation[11] so far fails to satisfactorily account for the observed chemical effects.

Motivated by these considerations, we have measured muonic x-ray intensities for a carefully chosen series of materials, selected with specific chemical structure factors in an attempt to observe simple trends in the capture process. Such x-ray measurements give the relative intensity ratios within the muon Lyman and Balmer series, as well as the total relative capture probabilities for the constituent atoms of the respective compounds.

The important target sequences were (1) the isoelectronic series Ar (liquid), KCl, and CaS (with Ca, S, and $CaSO_4$ for comparison); (2) $NaClO_4$, $MgSO_4$, $AlPO_4$, and SiO_2, an isoelectronic, isostructural series (which were compared with NaCl, $MgSO_4 \cdot 7H_2O$, and Si); although the overall crystal structure of these compounds is not the same, the local tetrahedral coordination of oxygens about a central atom is present in each with comparable bond lengths; and (3) a series of chlorides, NaCl, $MgCl_2$ (intended), and $AlCl_3$ (which were compared with KCl and $CaCl_2$). $MgCl_2$ was ultimately not run because it could not be obtained in anhydrous form. Also, ordinary tap water was briefly examined to compare with data for H_2O taken at the Los Alamos Meson Physics Facility (LAMPF).

II. EXPERIMENTAL PROCEDURE

The experimental work was performed at the 184-in. cyclotron of the Lawrence Berkeley Laboratory. The negative meson beam was produced in an internal Be target, and momentum analyzed by the fringing field of the cyclotron. It then exited from the machine through a thin window in the vacuum tank, and entered the meson cave through a 2-m-long collimator. In the meson cave the beam was directed to the counter telescope axis and focused on the target with a bending magnet and a quadrupole doublet. The nominal momentum of the extracted beam was 180 MeV/c, the minimum convenient value consistent with geometric constraints.

The counter telescope, target, and Ge(Li) detector rested on a large table mounted on rails so that it could be rolled in or out of the beam line. The muon counter telescope consisted of four scintillation counters (S_1, S_2, S_3, S_4), and a water Cerenkov counter (C). The Cerenkov counter was placed between S_1 and S_2, and the target was placed at a 45° angle to the beam line and sandwiched between S_3 and S_4 (Fig. 1). The signature of a stopping pion or muon was $S_1\bar{C}S_2S_3\bar{S}_4$. A remotely controllable, variable thickness, polyethylene absorber, just upstream of S_1 was adjusted to maxi-

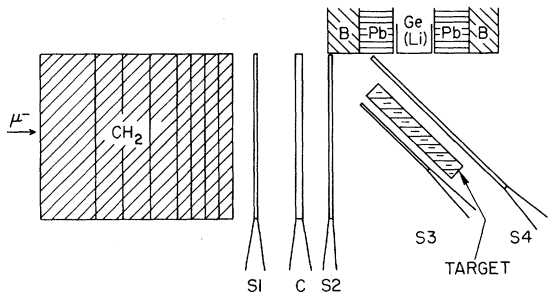

FIG. 1. Target arrangement. S_1, S_2, S_3, and S_4 are scintillation counters. C is a Cerenkov counter. CH_2 represents polyethylene degrader.

mize the stopping rate of muons in the target. Optimum absorber thickness was determined by maximizing the number of muonic $K\alpha$ x-rays detected in the Ge(Li) spectrometer per stopped particle. At this optimum absorber thickness the contamination from shorter-ranged pions was, for the purpose of this experiment, negligible.

The Ge(Li) crystal, 30-cm^3 active volume with true coaxial geometry, was set opposite the back face of the target at 90° to the beam line (and thus at 45° to the target). The distance from the front face of the Ge(Li) to the center of the target was about 11 cm. The detector was shielded with lead bricks to reduce photon background and also surrounded with boric acid bricks and sacks of borax to reduce neutron damage to the detector. The line of sight of the Ge(Li) detector to the target and the beam line, was shielded by the scintillator, S_4.

A requirement for a valid Ge(Li) pulse was the signal, $[\text{Ge(Li)}]\overline{S}_4$. This anticoincidence condition eliminated background due to muon-decay electrons from the target area. While redundant for the prompt x rays, this anticoincidence requirement was useful for reducing background in the comparison delayed-time spectra. The system resolution was approximately 3 keV at 1.33 MeV, compared to the detector's intrinsic resolution of 1.9 keV. The degradation of resolution resulted from the use of long cables and a short amplifier time constant, necessary to enable high data-acquisition rates.

Each signal from the Ge(Li) detector was routed through one of four contiguous time gates, depending on its time of arrival relative to a muon stop. Pulses in each gate were processed by an analog to digital converter (ADC) and stored in one of four 4096-channel pulse-height spectra, using a PDP-15 computer.

Prompt coincidences were centered in the second timing gate, G_2, of width 25 nsec. The spectrum addressed by this gate nominally contained the x-rays. The spectrum in the "negative time" gate, G_1, was comprised primarily of uncorrelated background, and the spectra in the two delayed gates, G_3 and G_4, primarily contained correlated delayed γ rays. Monitoring of the overflow of the x-ray spectra into G_1 and G_3 ensured against x-ray losses due to energy-dependent timing shifts. This precaution proved to be essential for yield determinations of the lower-energy L x rays because a timing shift did move a significant but determinable fraction of these x rays into G_3.

The electronic system accepted data only during the time of uniform cyclotron beam spill. The telescope pulses were also gated by a pile-up reject system. The gated muon stopping rate was 25×10^3 to 30×10^3 μ^-/sec.

The target materials were of commercial reagent-grade purity. The target holders were 8×8-in. Lucite frames, $1\frac{7}{8}$ in. thick with 0.010-in. Mylar windows. The target thicknesses were all approximately 5 g/cm^2.

The muonic x-ray intensities were determined by a version of the spectrum analysis code GAMANL,[12] which employs Fourier transforms for spectrum smoothing. In general, GAMANL worked accurately when compared with hand integrated spectra, except for a few of the lowest energy peaks near the discrimination threshold. Hand integrated intensities were employed for these cases. Uncertainties in area are those assigned by the GAMANL program. For the manually analyzed peaks, the statistical counting error was combined with an estimated uncertainty in the amplitude of the hand-drawn background baseline. In addition, intensities were corrected both for detector photopeak efficiency and x-ray absorption in the target.

The relative efficiency-versus-energy calibration for the Ge(Li) spectrometer was made using IAEA standards and ^{182}Ta, and employing the method described by Jardine.[13] This calibration was repeated *in situ* for the entire electronic system in addition to the Ge(Li) detector itself. The muon stopping signal was simulated by a fast signal generated from the Ge(Li) pulse. For energies above 250 keV the overall system efficiency was identical to that of the detector alone. However, at energies below 250 keV there was a significant relative fall off in the overall system efficiency. This was apparently due to the combined effects of time slewing and threshold jitters in the fast-slow coincidence network that generated the logic and timing pulses for the Ge(Li) detector. The *in situ* calibration was repeated at the beginning or end of each running period (one or two days). Efficiency calibration errors of ±3% were assigned for energies above 250 keV and of ± 10% for ener-

gies below 250 keV (this included the oxygen K x rays and almost all measured L x rays).

Target attenuation was calculated as a function of energy using the actual target geometry but assuming a point detector at the center of the face of the actual detector. Results were calculated both for a uniform stopping distribution and for a Gaussian that more nearly approximated the true distribution. The triple integrals were evaluated numerically by eight-point Gaussian quadrutures. Results from the two assumed stopping distributions were negligibly different. Attenuation corrections were as much as 46% at the lowest energies. However, the greatest relative correction over the range of any single K x-ray series was only 3% and only 12% over the range of an L series. No additional error was assigned to this target-attenuation correction. The internal consistency of the calibrations and corrections were checked for each element by comparing the Lyman-α intensity with the Balmer sum. These should be equal, and were found to be so, within the approximately 15% measurement uncertainty.

III. RESULTS AND DISCUSSION

Table I contains most of the measured muonic Lyman series intensity ratios. The tabulated uncertainties include statistical error and error from detector efficiency and self-absorption corrections. Additional analysis has modified some values we have previously published.[14] The data are in general agreement with other reported values[15,16] within the quoted uncertainties.

A striking result of this data is the marked similarity of the intensity patterns for the calcium ion in Ca metal, $CaCl_2$, CaS, and $CaSO_4$, for the sodium ion in NaCl, and $NaClO_4$, and for the chloride ion in NaCl, KCl, $CaCl_2$, and $AlCl_3$. The data for the calcium ion is shown in Fig. 2. Very recent data[17] taken at LAMPF for Na, and K shows intensity patterns similar to those we report here for these elements in NaCl and KCl. These observations suggest that for alkali and alkaline earth metals and ionic compounds of these elements, muons are captured by a given ionic species with the same initial angular momentum dis-

TABLE I. Lyman series intensity ratios ($\times 10^3$).

Element	Target	$K\beta/K\alpha$	$K\gamma/K\alpha$	$K\delta/K\alpha$	$K\epsilon/K\alpha$	$K\zeta/K\alpha$	$K\eta/K\alpha$	$K\theta/K\alpha$
Na	NaCl	100±11	71±9	42±6	18±5			
	$NaClO_4$	112±13	79±10	47±8	19±6			
Mg	$MgSO_4$	108±7	56±6	48±6	11±5			
	$MgSO_4 \cdot 7H_2O$	119±13	67±13	61±11	17±11			
Al	$AlCl_3$	73±5	43±5	39±5				
	$AlPO_4$	102±8	55±7	53±7	49±12			
Si	Intrinsic	82±3	48±2	35±2	22±1	8±1		
	SiO_2	81±4	42±3	31±3	20±2	8±2		
P	$AlPO_4$	73±6	51±6	46±6	27±6	11±6		
S	CaS	89±7	25±5	23±5	16±5	7±4		
	$CaSO_4$[a]	89±9	37±7	34±6	22±6	9±5		
	$MgSO_4$	79±6	37±5	37±5	33±5			
	$MgSO_4 \cdot 7H_2O$	90±19	41±13	49±12	28±13			
	S rhombic	79±3	39±3	45±2	30±2	20±2	7±2	5±2
Cl	NaCl[a]	73±4	23±3	28±3	20±3	9±3		
	KCl	81±5	23±4	24±4	15±4	4±3		
	$CaCl_2$	73±3	31±2	28±2	23±2	10±2		
	$AlCl_3$	76±3	31±1	31±1	24±2	14±2		
	$NaClO_4$[a]	93±6	43±5	45±5	36±4	24±4		
Ar	Liquid	73±4	20±3	23±3	21±3	12±3	12±3	
K	KCl	73±4	28±3	29±4	26±3	13±3	10±4	7±4
Ca	Metal	79±3	25±2	25±2	23±2	15±2	12±2	2±1
	CaS	64±4	22±4	23±4	19±4	8±4		
	$CaCl_2$	64±4	22±3	26±3	18±3	12±3		
	$CaSO_4$	76±5	27±5	22±6	20±5	12±4	13±6	

[a] Ratios modified from those reported in Ref. 14.

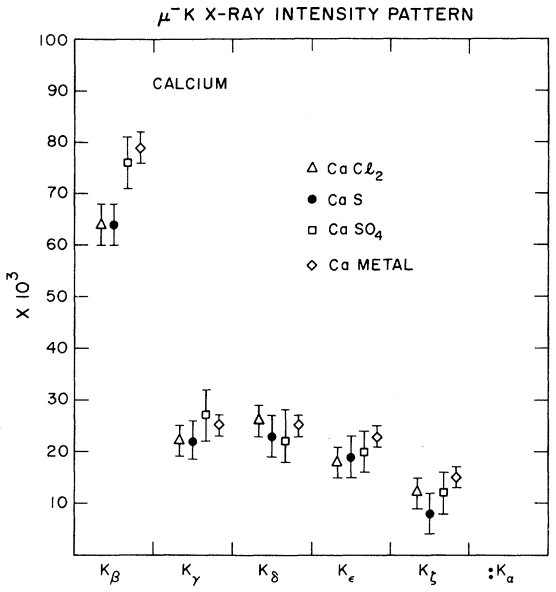

FIG. 2. Ratio of Lyman series intensities to the $K\alpha$ intensity for calcium (e.g., $K\beta/K\alpha$, $K\gamma/K\alpha$ etc.).

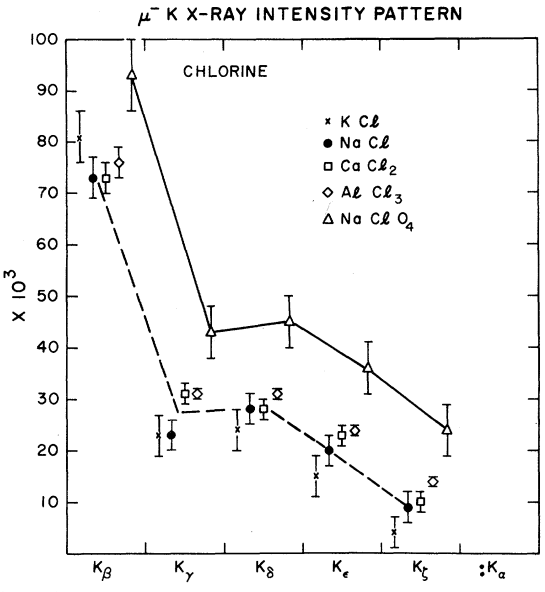

FIG. 3. Lyman series ratios for chlorine. The lines are drawn only to guide the eye.

tribution. We note that for these ions the electron distribution is isotropic. Thus the angular momentum distribution is apparently not significantly influenced by such factors as the bond partner, gross crystal structure (e.g., face centered cubic for Ca but orthorhombic for $CaSO_4$), electrical resistivity (e.g., about 10^{-6} Ω cm for Ca compared to about 10^{16}-10^{22} Ω cm for alkali halides) and band gap (about 8 eV for alkali halides and none for metals). Since electron vacancies can have a large effect on the muon cascade this insensitivity to variation in electrical resistivity may imply that the time required for electrons to refill the electronic shells of the capturing ion (depleted by the muonic Auger effect) is not significantly different for metals and insulators, or is short compared to the cascade time.

Clear evidence of the influence of chemical structure on the muon capture mechanism is manifest in the comparison of the intensity ratios of the ionic chlorides (Cl^-) with the covalent chlorine (formal valence Cl^{+7}) in $NaClO_4$. The differences in these ratios are shown in Fig. 3. The higher members of the Lyman series are more intense by up to a factor of 2 for the covalently bonded chlorine. A similar chemical difference is apparent between the intensity pattern of the sulfide ion (S^{-2}) in CaS and the pattern of pure rhombic sulfur (cyclic S_8 molecules) and sulfur (formally S^{+6}) in $CaSO_4$ and $MgSO_4$ (see Fig. 4). Again the covalent species yields intensity ratios enhanced by almost a factor of 2. The higher members of the Lyman series have also been observed by Knight *et al.*[15] to gain intensity on progression through a series of strongly ionic to strongly covalent metal oxide targets. One may speculate that this difference between ionic and covalent compounds is related to the shape of the electron distribution about each atom. Unlike the isotropic electron distribution

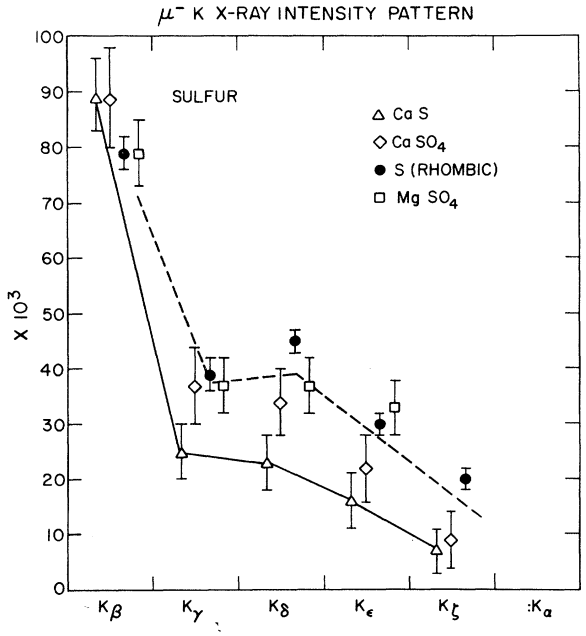

FIG. 4. Lyman series ratios for sulfur. The lines are drawn only to guide the eye.

for ionic species, the electron distribution in covalent bonds is directed along the bond axes. Further, this effect emphasizes the influence of valence electrons, as opposed to the core, on the muon capture mechanism.

From Table I we may also compare the Lyman intensity ratios for the $MgSO_4$ and $MgSO_4 \cdot 7H_2O$ targets. The ratios appear somewhat higher for both Mg and S in the hydrate. This may be due to the possible formation of the p-μ "pseudoneutron." This structure is known to transfer muons to high Z nuclei with low angular momentum and attendant increased strength in the higher Lyman series members.[18-21] The data are suggestive of this effect but better statistics are needed to provide firmer evidence.

The intensity data for intrinsic silicon and silicon in SiO_2 also appears in Table I. The Si intensity patterns are quite similar. These are both covalent crystals where Si has sp^3 orbital hybridization.

Chemical effects are also manifest in the similarity of the oxygen Lyman spectra in the series $NaClO_4$, $MgSO_4$, $CaSO_4$, $AlPO_4$, and SiO_2 (Table II). In all of these compounds the oxygens are tetrahedrally placed about a central atom with similar bond lengths. Our water data (Table II) are in fair agreement with previous measurements.[15,22]

The Balmer series results are shown in Table III. Our apparatus could not resolve radiation below about 100 keV so only the Balmer series spectra for Cl, Ar, K, and Ca were measured. We observed the same correlations for the Balmer intensity patterns as for the Lyman series. All of the calcium-ion spectra are roughly similar and all the chloride ion spectra are similar. Again, the higher members of the series are more intense for chlorine in $NaClO_4$ than for the chlorides.

TABLE II. Oxygen Lyman intensity ratios ($\times 10^3$).

Element	Target	$K\beta/K\alpha$	$K\gamma/K\alpha$	$K\delta/K\alpha$
O	$NaClO_4$	275±41	226±35	136±21
O	$MgSO_4$[a]	269±42	205±32	84±14
O	$MgSO_4 \cdot 7H_2O$[a]	283±43	222±33	134±21
O	$CaSO_4$[a]	261±40[b]	210±32	118±19
O	$AlPO_4$	287±43	225±34	135±21
O	SiO_2	280±42	181±27	67±10
O	H_2O	268±45	220±35	93±17

[a] Oxygen $K\alpha$ could not be resolved from sulfur $L\beta$. The oxygen intensity was obtained by using the oxygen $K\delta/K\alpha$ ratio in $AlPO_4$.

[b] Oxygen $K\beta$ could not be resolved from calcium $L\alpha$. The intensity was obtained from the oxygen $K\delta/K\beta$ ratio in $AlPO_4$.

TABLE III. Balmer series intensity ratios ($\times 10^3$).

Element	Target	$L\beta/L\alpha$	$L\gamma/L\alpha$	$L\delta/L\alpha$	$L\epsilon/L\alpha$
Cl	NaCl	150±23	74±13	27±7	18±7
	KCl	153±23	63±11	19±6	
	$CaCl_2$	150±22	76±11	26±4	9±2
	$AlCl_3$	177±26	92±13	31±5	9±2
	$NaClO_4$	150±29	111±19	70±16	19±11
Ca	Metal	109±16	46±7	25±4	17±3
	CaS	135±20	52±8	12±4	
	$CaSO_4$	119±19	49±8	28±5	13±4
	$CaCl_2$	110±12	44±5	10±2	7±3
K	KCl	128±19	55±9	41±7	17±4
Ar	Liquid	177±27	62±10	28±6	11±4

The measured intensities may be compared to those calculated with a cascade model of muon deexcitation,[11] which assumes a certain muon initial angular momentum distribution at some muon principal quantum number (usually 14–20). For convenience, a modified statistical distribution of the form $P(l) = (2l+1)\, e^{\alpha l}$ is usually chosen. The parameter α is varied to obtain the best fit to the data. The calculations were performed with the computer code CASCADE.[23] The parameter α was varied in steps of 0.10. Each x-ray spectrum calculated in this way was compared to the experimental spectrum and the reduced chi-square (χ^2_ν) was determined. The range of α spanned the minimum value of χ^2_ν. Table IV gives the values of α corresponding to the lowest χ^2_ν found, along with those χ^2_ν values. In addition, χ^2_ν is shown corresponding to values of α bracketing the minimum. Some of the χ^2_ν values are quite large, but this does not reveal the details of the quality of the fit. Figure 5 shows the data for chlorine in $CaCl_2$ compared with the calculated intensity ratios for $\alpha = +0.2$ and $+0.3$. We see that the $K\beta/K\alpha$ and $K\gamma/K\alpha$ ratios may be fitted with $\alpha = +0.3$. However, at $K\delta/K\alpha$ the data lies between the calculated points. Agreement for the $K\epsilon/K\alpha$ and $K\zeta/K\alpha$ ratios required $\alpha = +0.2$. This required variation in α was observed for almost all targets employed. If the cascade was started at different initial principal quantum numbers ($N\mu = 15$, 16, 17, 18), negligible variation in the calculated intensity ratios was predicted by the code. Allowing for K-shell electron vacancies significantly depressed the calculated ratios, nevertheless, no single value of α could reproduce the appropriate intensity patterns. It should be noted, therefore, that while the $(2l+1)\, e^{\alpha l}$ distribution is customarily chosen for calculational convenience it does not appear to reflect an actual initial distribution of the captured muons.

By summing the intensities of all observed Ly-

TABLE IV. Fitting parameters for calculated spectra.

Element	Target	α	$\chi^2_\nu(\alpha - 0.1)$	χ^2_ν(min.)	$\chi^2_\nu(\alpha + 0.1)$
Na	NaCl	0.3	12.1	2.9	21.1
	$NaClO_4$	0.3	4.8	1.9	7.2
Al	$AlCl_3$	0.4	17.3	8.3	15.5
	$AlPO_4$	0.3	5.9	5.4	13.5
Si	Si	0.3	51.1	18.5	36.1
	SiO_2	0.3	37.9	4.1	10.0
P	$AlPO_4$	0.2	19.1	4.6	10.8
S	S	0.2	66.5	10.5	25.7
	$CaSO_4$	0.2	16.0	1.1	1.2
	$MgSO_4$	0.2	18.3	3.7	5.9
	$MgSO_4 \cdot 7H_2O$	0.2	2.6	0.3	1.8
	CaS	0.3	9.2	1.9	3.8
Cl	NaCl	0.3	15.6	4.6	10.9
	$AlCl_3$	0.3	40.3	22.9	150.8
	KCl	0.3	11.1	2.3	5.7
	$CaCl_2$	0.3	17.9	8.6	33.0
	$NaClO_4$	0.2	6.4	5.8	21.3
Ar	Ar (liquid)	0.3	21.4	8.3	9.1
Ca	Ca (metal)	0.2	35.6	4.0	17.7
	CaS	0.3	8.4	1.3	5.4
	$CaSO_4$	0.2	2.8	2.0	8.8
	$CaCl_2$	0.3	9.1	4.1	11.6

TABLE V. Relative muon capture probabilities.

Compound $Z_mZ'_k(O_4)$	Capture ratio $A(Z/Z')$ Expt.	Other expts.	Z law	Other calcs.
NaCl	0.684 ± 0.058	0.787 ± 0.031 [a]	0.647	0.699 [d] 0.731 ± 0.072 [e]
$NaClO_4$	0.698 ± 0.059		0.647	
KCl	1.16 ± 0.03	1.15 ± 0.05 [a]	1.12	1.09 [d] 1.34 ± 0.14 [e]
$CaCl_2$	1.27 ± 0.03	1.56 ± 0.17 [b]	1.18	1.13 [d]
CaS	1.57 ± 0.04		1.25	1.18 [d] 1.31 ± 0.18 [e]
$CaSO_4$	1.89 ± 0.06		1.25	
$MgSO_4$	0.829 ± 0.022		0.750	
$MgSO_4 \cdot 7H_2O$	0.923 ± 0.040		0.750	
$AlCl_3$	0.662 ± 0.016	0.63 ± 0.21 [c]	0.765	0.81 [d]
$AlPO_4$	0.888 ± 0.026		0.867	
SiO_2	0.865 ± 0.066	0.79 ± 0.07 [b]	1.75	1.65 [d]

[a] Reference 15.
[b] Reference 24.
[c] Reference 25.
[d] Reference 26.
[e] Reference 27.

man series transitions we can determine the relative muon capture probabilities $W(Z)$ and $W(Z')$ for the elements Z and Z' in the compound $Z_m Z'_k$. Then the atomic capture ratios is given as

$$A(Z/Z') = \frac{W(Z)/m}{W(Z')/k} .$$

In Table V, $A(Z/Z')$ from this work is compared with other measurements as well as with the predictions of the Fermi-Teller Z law and more recent calculations. The agreement with reported values for NaCl, KCl, $AlCl_3$, and SiO_2 is generally satisfactory. The predictions from the modified Z law of Daniel[26] and the Monte Carlo method of Vogel *et al.*[27] fit the data about as well as the Z law. However, Vogel *et al.* probably would have achieved better agreement with experiment by using more realistic ionicity values. The large deviation from the Z-law ratio for SiO_2 is in agreement with previous observations[15,24] that the relative capture probability by oxygen is always enhanced; a result that has been attributed to the large electronegativity (muon affinity?) of oxygen. The deviation of $A(Ca/S)$ in CaS and $CaSO_4$ has been noted previously.[14]

We wish to express our gratitude to the technical staff of the 184 in. Cyclotron for their cooperation and assistance in setting up and running these experiments. We also would like to acknowledge many helpful discussions with Dr. Jere D. Knight of the Los Alamos Scientific Laboratory in connection with this work.

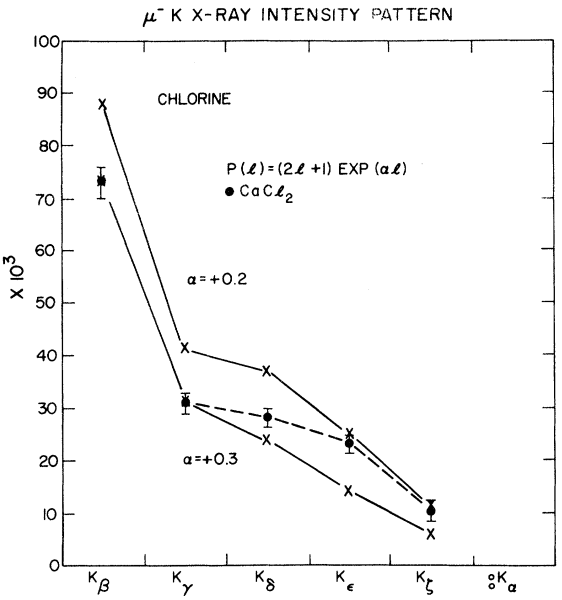

FIG. 5. Calculated intensity ratios of chlorine in $CaCl_2$.

*Work supported by U.S. Energy Research and Development Administration.

†Present address: Los Alamos Scientific Laboratory, Los Alamos, N.M. 87545. Work in partial fulfillment of the requirements for the Ph.D. degree, Princeton University.

‡Present address: General Electric Co., NED, San Jose, Calif. 95125.

[1]S. S. Gershtein, V. I. Petrukhin, L. I. Ponomarev, and Yu. D. Prokoshkin, Usp. Fiz. Nauk, 97, 3 (1969) [Sov. Phys. Usp. 12, 1 (1969)].

[2]Y. N. Kim, *Mesic Atoms and Nuclear Structure* (American Elsevier, New York, 1971).

[3]L. I. Ponomarev, Annu. Rev. Nucl. Sci. 23, 395 (1973).

[4]L. I. Ponomarev, in *Proceedings of the Sixth International Conference on High Energy Physics and Nuclear Structure, Santa Fe and Los Alamos, 1975,* AIP Conference Proceedings No. 26, edited by D. E. Nagle, A. S. Goldhaber, C. K. Hargrove, R. L. Burman, and B. G. Storms (American Institute of Physics, New York, 1975).

[5]S. S. Gershtein and L. I. Ponomarev, in *Muon Physics,* edited by V. W. Hughes and C. S. Wu (Academic, New York, 1975), Vol. 3, Chap. VII, Sec. 2.

[6]V. S. Evseev, in *Muon Physics,* edited by V. W. Hughes and C. S. Wu (Academic, New York, 1975), Vol. 3, Chap. VII. Sec. 3.

[7]E. Fermi and E. Teller, Phys. Rev. 72, 399 (1947).

[8]M. Y. Au-Yang and M. L. Cohen, Phys. Rev. 174, 468 (1968).

[9]M. Leon and R. Seki, Phys. Rev. Lett. 32, 132 (1974).

[10]P. K. Haff, P. Vogel, and A. Winther, Phys. Rev. A 10, 1430 (1974).

[11]Y. Eisenberg and D. Kessler, Nuovo Cimento 19, 1195 (1961); Phys. Rev. 123, 1472 (1961).

[12]T. Harper, T. Inouye, N. C. Rasmussen, MIT Report No. MIT-3944-2, MITNE-97, 1968 (unpublished).

[13]L. J. Jardine, Nucl. Instrum. Methods 96, 259 (1971).

[14]L. F. Mausner, R. A. Naumann, J. A. Monard, and S. N. Kaplan, Phys. Lett. 56B, 145 (1975).

[15]J. D. Knight, C. J. Orth, M. E. Schillaci, R. A. Naumann, H. Daniel, K. Springer, H. B. Knowles, Phys. Rev. A 13, 43 (1976).

[16]A. Suzuki, Phys. Rev. Lett. 19, 1005 (1967).

[17]Los Alamos Meson Physics Facility, experiment 60 (unpublished).

[18]Yu. G. Budyashov, P. F. Ermolov, V. G. Zinov, A. D. Konin, and A. I. Mukhin, Sov. J. Nucl. Phys. 5, 426 (1967).

[19]G. Backenstoss, H. Daniel, K. Jentzsch, H. Koch, H. P. Povel, F. Schmiessner, K. Springer, and R. L. Stearns, Phys. Lett. 36B, 422 (1971).

[20]H. Daniel, H. J. Pfeiffer, and K. Springer, Phys. Lett. 44A, 447 (1973).

[21]G. Holzwarth and H. J. Pfeiffer, Z. Phys. 272, 311 (1975).

[22]H. Koch, Ph.D. thesis, University of Karlsruhe, 1969, as cited by A. B. D'Oliveira, H. Daniel, and T. Von Egidy, Lett. Nuovo Cimento 10, 197 (1974).

[23]J. Hufner, Z. Phys. 195, 365 (1966), and Computer Program CASCADE (CERN, Geneva).
[24]V. G. Zinov, A. D. Konin, and A. I. Mukhin, Sov. J. Nucl. Phys. 2, 613 (1966).
[25]A. Brandao d'Oliveira, H. Daniel, and T. von Egidy, Phys. Rev. A 13, 1772 (1976).
[26]H. Daniel, Phys. Rev. Lett. 35, 1649 (1975).
[27]P. Vogel, P. Haff, V. Akylas, and A. Winther, Nucl. Phys. A 254, 445 (1975).